

## "CHIP-SIZE" ANTENNAS FOR IMPLANTABLE SENSORS AND SMART DUST

P. Basset<sup>1,4</sup>, F. Alfaro<sup>2</sup>, D. Novosel<sup>3</sup>, A. de la Plaza<sup>3</sup>, D. Stancil<sup>1</sup> and G. K. Fedder<sup>1,2</sup>

<sup>1</sup>Carnegie Mellon University - Department of Electrical and Computing Engineering - USA

<sup>2</sup>Carnegie Mellon University - The Robotic Institute - USA

<sup>3</sup>Novocell Semiconductor - USA

<sup>4</sup>now at ESYCOM-ESIEE - France

e-mail: p.basset@esiee.fr

### ABSTRACT

In this paper, we present the analysis, design and experimental results of  $\lambda/4$ -patch antennas operating at  $\sim 10$  GHz. The ground plane has been adjusted to the patch area in order to drastically reduce the antenna size. Several geometries are presented, with HFSS simulation results. Impedance matching calculations for maximum power transfer between the antenna and the rectifying circuit is also presented. For a  $4 \times 5 \times 1.6$  mm<sup>3</sup> rectangular antenna fabricated on a RT/Duroid 5880 Printed Circuit Board (PCB), the measured maximum gain is 0.75 dB<sub>i</sub> at 10.3 GHz.

**Keywords:** Microstrip antenna, implantable sensors.

### INTRODUCTION

The need to transfer measured data with a wireless link has become more important given the increase of microsystems for sensor applications. Some examples include biomedical monitoring, distributed sensors within civil engineering and sensors implanted within the body. This paper presents initial work to develop the technology to enable fabrication of a complete wireless sensor chip. The final goal is to provide wireless communication and powering of sensors integrated completely on chip.

An example of such a chip for a medical application is shown in Figure 1. The sensor requires an integrated antenna for reception of power and transmission of data. At the reception, the antenna signal is rectified and regulated to power the system on chip. Data from the transducer is transmitted to an external base station via the same antenna.

Several similar systems have already been investigated by different groups, but a full integrated chip hasn't been achieved so far, mainly because of the requirements of a small size antenna. Recent work [1] shows data communication at microwave frequencies (1-3 GHz) using a pair of external (25 x 25 mm) and internal (6 x 6 mm) microstrip patch antennas. This paper presents the work done in the design of a microstrip antenna operating at a frequency of 10 GHz, with an area size as small as 5x5 mm<sup>2</sup>. Microstrip antennas can be

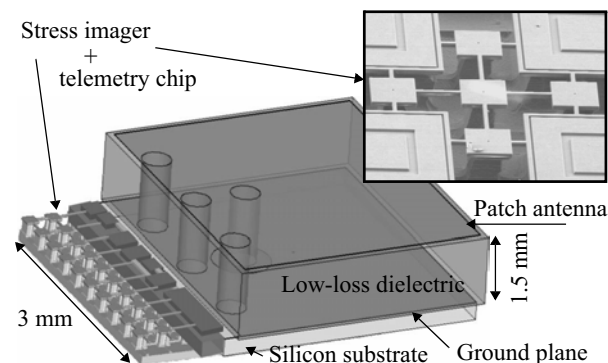


Figure 1 : Integrated implantable bone sensor concept with SEM of the stress imager prototype. Final goal is to fabricate the antenna on top of the RF-chip.

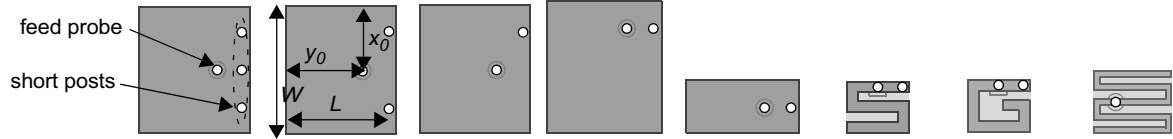
used in any application which requires high-performance, compact, low-cost planar antennas such as imaging arrays, collision avoidance radars.

### ANTENNA DESIGN

A  $\lambda/2$ -patch is equivalent to an array of two magnetic dipoles of same orientation and spaced by  $\lambda/2$ , where no power is radiated on the backside thanks to an infinite ground plane below the radiating element [2]. This yields a pattern where the maximum directivity is at the patch zenith ( $\theta=0$ ). A similar resonance can be obtained, by using the method of image, if a perfect electric conductor is located at a distance of  $\lambda/4$  from the first radiating edge. This principle is used to divide by two the antenna's length. The "array effect" of the two radiating edges disappeared and the radiation pattern in the E-plane becomes broader. The maximum directivity occurs at the horizon ( $\theta = \pm 90^\circ$ ) and the antenna acts like a short monopole [3].

#### Ground plane size reduction

To obtain a printed "chip-size" antenna, the ground plane has to be drastically reduced. This reduction will have two major consequences. First, backside radiation will appear, leading to a decrease of directivity in the forward direction. Second, the frequency will increase compared to an identical patch with an infinite ground plane. The slope of this frequency shift becomes very

Table 1: HFSS simulations results of various antenna designs on a RT/Duroid 5880 substrate ( $\epsilon_r=2.2$ )

Design:	#1	#2	#3	#4	#5	#6	#7	#8
$W*L$ (mm <sup>2</sup> )	5*4	5*4	5*4	5*4	2*4	2*2.4	2*2.4	2.6*3
$(x_0, y_0)$ (mm)	(2.5, 3)	(2.5, 3)	(1, 3)	(2.5, 3)	(1, 3)	(0.2*1.6)	(0.2*1.2)	(1.3*0.8)
$f_0$ (GHz)	10.75	10	7.25	7	10.35	10.75	10.3	10.7
Gain (dBi)	1.8	1.6	0.24	0.12	1.4	0.86	0.45	0.59
	@ 11 GHz	@ 10 GHz	@ 7 GHz	@ 7 GHz	@ 10 GHz	@ 11 GHz	@ 10 GHz	@ 10.5 GHz
$Z_{in}$ @ $f_0$ ( $\Omega$ )	$\sim 450+j70$	$\sim 1000+j70$	$\sim 1500$	$\sim 3750$	$\sim 2750$	$\sim 3700$	$\sim 3500$	$\sim 200$

large when the ground plane size is of the same order than the patch itself [4]. At that point the antenna's characteristics are very sensitive to the fabrication process accuracy. With a  $\lambda/4$ -patch, the peak directivity directions vary when the ground plane size decreases and is at the horizon when it is at the same size as the upper plate. The patch is then acting like a short dipole [3].

### Antenna geometry

Several geometries of  $\lambda/4$ -printed antennas without a ground plane rim have been simulated with HFSS [5] using conventional RF printed-circuit technology. A summary of the results is presented in Table 1. The  $\lambda/4$ -patch can be obtained by using a number of pins or plated vias connected between the patch metallization and the ground plane. The patch length must be adjusted to account for the Short-Post (SP)'s reactance. Reducing the number of SP reduces the resonant frequency (the added capacitance decreases) and reduces the electrical conductivity between the feed point and the ground plane of the microstrip antenna, which increases the input resistance [6].

A *Planar Inverted-F Antenna* (PIFA) is a 1-post loaded rectangular microstrip antenna fed by a probe (ant. #3, #4 and #5 in table 1). It is called an *inverted-F* antenna because its side view resembles the letter F with its face down. If the patch's width is much larger than the SP's diameter, the post is no longer located at a zero electric field position but at a radiating edge [7]. Orthogonal cross polarizations (TM<sub>10</sub> and TM<sub>01</sub> resonance) occur, yielding a lower gain and bandwidth. Maximum reduction in the size of the antenna is achieved when the short is located at the corner of the patch. Approximately, the resonant frequency is now determined by the perimeter of the patch rather than the length  $L$ . The approximate expression for the resonant frequency  $f_r$  is given by (with infinite ground plane) [8]:

$$f_r = \frac{1}{4} \frac{c}{\sqrt{\epsilon_r}(L+W)} \quad (1)$$

Some publications have used meander PIFAs with S

[9] (ant. #6) and G [10] (ant. #7) shapes to reduce the size of the antenna. Increasing the number of segments decreases the resonant frequency but the efficiency too, since the main losses appear in the corners [9]. If a low input impedance is needed and hardly feasible because of the manufacturer's design rules, a  $\lambda/2$  S-Shape meander dipole can be used (ant. #8).

### POWER TRANSFER

It is well known that maximum power transfer is obtained for conjugate matching between the source impedance  $Z_s=R_s+jX_s$  and the load impedance  $Z_l=R_l+jX_l$ . The power available across  $Z_l$  is given by:

$$P_l = \frac{V_s^2}{8R_s} \cdot (1-|\rho|^2), \quad \rho = \frac{Z_l - Z_s^*}{Z_l + Z_s} \quad (2)$$

where  $V_s$  is the source voltage and  $\rho$  the reflection coefficient.

With a wire antenna as a source,  $R_s$  at resonance would be equal to the radiation resistance  $R_{rad}$  (in serial with the ohmic and dielectric losses). But with a patch antenna,  $R_s$  is less than or equal to  $R_{rad}$ , depending on the feed location  $(x_0, y_0)$  [2].  $X_s$  is mainly due to the probe diameter and usually much smaller than  $R_{rad}$ .  $V_s$  is then the voltage between the patch and the ground plane at  $(x_0, y_0)$ , and is equal to, for a  $\lambda/2$ -patch:

$$V_s(y_0) = -E(x_0, y_0) \int_0^h dz = -h \cdot E_0 \cos\left(\frac{\pi y_0}{L}\right) \quad (3)$$

where  $E_0$  is the peak of the received electric field.  $V_s$  is maximum at the radiating edges and decreases in a similar way that  $R_s$ . There is a trade off with the need to have a high value for  $R_s$  to get enough voltage to overcome the threshold of the rectifier's input diodes, and to have a low  $R_s$  to maximize the available power.

### The regulated rectifier

In order to use the chip at any frequency, no impedance matching circuit is implemented so we are dependent on the input impedance of the rectifier. The

circuit is based on a typical Cockcroft-Walton architecture and its schematic is represented in Figure 2. A regulated output is obtained by applying a DC voltage on the gate of transistors  $T_1$  and  $T_3$  instead of using them as simple diodes. Since the applied voltage is dependant on the DC-output, when  $V_{out}$  increases, the  $V_{be}$  of  $T_1$  and  $T_3$  decrease.

From a Spectre transient simulation, an FFT of the input voltage and current has been performed to determine their real and imaginary parts, and then combined to determine the complex input impedance of the circuit  $Z_{in}$ . Figure 3 shows  $Z_{in}$  and the regulated output for 3 different input voltages  $V_{in,peak}$  (with the Jazz SiGe 60GHz process). For small voltages,  $Z_{in}$  is mainly reactive, but the input capacitance increases with the increasing input voltage; the non-linearity in the transistors increases and then the real part of  $Z_{in}$  becomes predominant.

**Impedance matching**

For small received power,  $Z_{in}$  is in the order of  $130-j*380 \Omega$ . The real part can be easily matched, except that for a thin patch,  $R_{rad}$  can be above a few  $k\Omega$  and manufacturing issues can be important to obtain much smaller values. However, the imaginary part due to the probe is limited by its minimum diameter and from HFFS simulations, is around a few tens of ohms for the Duroid substrate. So perfect matching is not possible. In that case, maximum power transfer occurs when the magnitude of the reflection coefficient  $\rho$  is minimum. Since the input impedance of the rectifier is capacitive ( $X_l < 0$ ), the  $S_{11}$  will be minimum at a slightly lower frequency, where the impedance of the antenna has a positive imaginary part ( $X_s > 0$ ).

**EXPERIMENTAL RESULTS**

**Setup and measurement**

The experiment's setup is described in Figure 4. The measurement was performed by a spectrum analyzer that measured only the amplitude of the received signal. Figure 5 shows the measured pattern in the E and H planes of a  $4 \times 5 \times 1.6 \text{ mm}^3$  rectangular antenna (ant. #2)

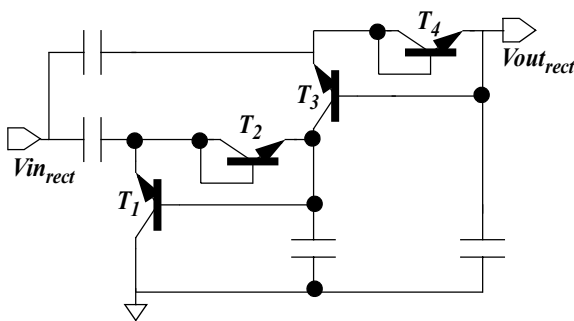


Figure 2 : Rectifier schematic with a regulated output

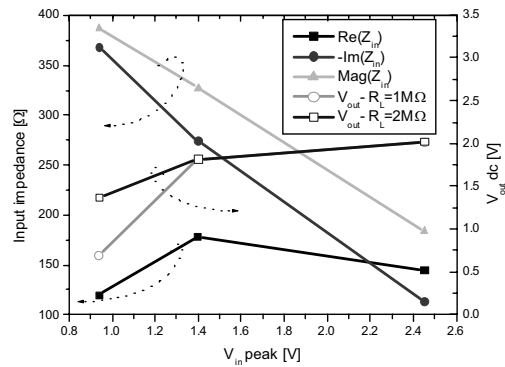


Figure 3 : Input impedance and regulated output of the rectifier versus peak input voltage ( $f_0=10 \text{ GHz}$ )

fabricated on RT/Duroid 5880 ( $\epsilon_r=2.2$ ). The maximum real gain appears at 10.3 GHz in the E-plane and its measured value is 0.58  $\text{dB}_i$ . At 10.2 GHz, the max gain is 0.24  $\text{dB}_i$  in the E-plane and -2.5  $\text{dB}_i$  in the H-plane. At 10.3 GHz, the  $S_{11}$  has been measured around -7  $\text{dB}_i$ . This low value is due to the mismatch with the 50  $\Omega$  cable. The gain of the antenna is then  $1.14/(1-.2^2) = 1.19 = 0.75 \text{ dB}_i$ . This is only 1  $\text{dB}_i$  less than the simulated directivity. There is also a  $45^\circ$  shift of the direction of maximum radiation. This can be explained by the ground plane size that is bigger (and irregular) than the simulated patch, which could also explained that the maximum gain occurs at a frequency above the simulated resonant frequency.

**Communication distance**

From the Friis formula [2], the propagation loss is (far field transmission):

$$\text{loss}[\text{dB}] = 20 \cdot \text{Log}\left(\frac{4\pi D}{\lambda}\right) - 10 \cdot \text{Log}G_t - 10 \cdot \text{Log}G_r \quad (4)$$

where  $D$  is the distance between the antennas,  $G_t$  and  $G_r$  the real gain (i.e. including matching loss) of the transmitting and receiving antennas, respectively.

Assuming the consumption of the receiver circuit  $P_r$ ,

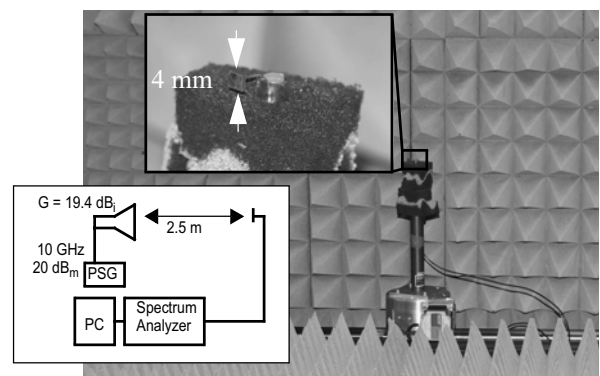


Figure 4 : Pattern measurement: setup schematic and picture of the experiment.

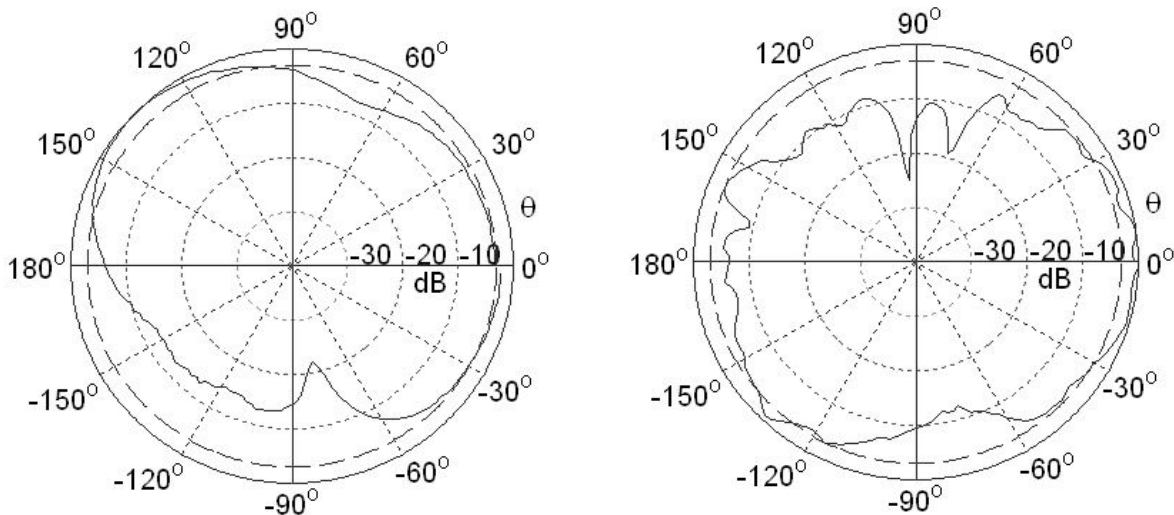


Figure 5 : Normalized pattern in the E and H planes of antenna B at 10.2 GHz.

is  $1 \mu\text{W}$ , for an isotropic antenna that radiates  $P_t=1$   $\text{W}_{\text{EIRP}}$  (Equivalent Isotropic Radiated Power) at the base station and the tested antenna as the tag, from (4) the maximum transmission distance  $D_{\text{max}}$  in free space would be:

$$D_{\text{max}} = \frac{\lambda}{4\pi} 10^{\left(\frac{P_r[\text{dB}_m] - P_t[\text{dB}_m] + G_r[\text{dB}_i] + G_t[\text{dB}_i]}{20}\right)} = 2.6 \text{ m} \quad (5)$$

## CONCLUSION

This paper presents a  $\lambda/4$ -patch antenna especially designed for sensor applications. Its small size allows an antenna on chip technology to produce very miniaturized telemetry devices. A  $4 \times 5 \times 1.6 \text{ mm}^3$  rectangular antenna has been fabricated on a RT/Duroid 5880 PCB. At 10.3 GHz, the maximum gain is  $0.75 \text{ dB}_i$ . Compared to the simulation's results, a  $45^\circ$  shift of the direction of maximum radiation has been observed, probably caused by a bigger and irregular ground plane than the simulated antenna.

Even though the operating frequency of 10 GHz was selected to minimize the antenna area, preliminary data have shown that power radiated at this frequency is highly attenuated within a couple of millimeters inside the body tissues. Also, IEEE standards for safety levels for human exposures to electromagnetic energy at GHz frequencies require a maximum exposure of  $10 \text{ mW/cm}^2$ , which limits the maximum power transmitted to an implantable antenna on chip. Therefore, this approach is useful outside the body but future work points to reduction of frequency while maintaining chip-size form factor.

## ACKNOWLEDGEMENT

The authors would like to thanks J. P. Van't Hof for the experiment's setup, as well as T. Mukherjee and

C. P. Yue.

## REFERENCES

- [1] K. Gosalia, G. Lazzi and M. Humayun, "Investigation of a Microwave Data Telemetry Link for a Retinal Prosthesis", *IEEE Transaction on Microwave Theory and Techniques*, vol. 52, n°8, 2004, pp. 1925-1933.
- [2] C. A. Balanis, "Antenna theory: analysis and design", 2nd edition, J. Wiley & sons ed., 1997.
- [3] M. C. Huynh *et al.*, "Ground plane effect on planar inverted-F antenna (PIFA) performance", *IEE Proceeding of microwave antennas and propagations*, vol. 150, n°4, 2003, pp. 209-213.
- [4] E. Lier *et al.*, "Rectangular microstrip patch antennas with infinite and finite ground plane dimensions", *IEEE Transactions on Antennas and Propagation*, vol. AP-31, n°6, 1983, pp. 978-984.
- [5] HFSS, High Frequency Simulation Software. <http://www.ansoft.com/products/hf/hfss/>, Ansoft Corporation.
- [6] M. Sanad, "Effect of the shorting posts on short circuit microstrip antenna", *IEEE Antenna and Propagation Society International Symposium*, 1994, pp. 794-796.
- [7] K. L. Wong *et al.*, "Compact microstrip antenna with dual-frequency operation", *Electronics Letters*, vol. 33, n°8, 1997, pp. 646-647.
- [8] R. Garg and *al.*, "Microstrip antenna design handbook", Artech House ed., 2001, p. 602.
- [9] H. Y. Wang, S. Taylor, J. Simkin, J.M. Oakley, C. Emson and M. J. Lancaster, "Simulation of microstrip small antennas", *IEE Int. Conf. in Antennas and propagation*, 2001, pp. 611-614.
- [10] J. Kim *et al.*, "Implanted Antennas Inside a Human Body: Simulations, Designs, and Characterizations", *IEEE Transaction on Microwave Theory and Techniques*, vol. 52, n°8, 2004, pp. 1934-1943.
- [11] K. Gosalia, G. Lazzi and M. Humayun, "Investigation of a Microwave Data Telemetry Link for a Retinal Prosthesis", *IEEE Transaction on Microwave Theory and Techniques*, vol. 52, n°8, 2004, pp. 1925-1933.